

The dynamics of starvation and recovery

2 Justin D. Yeakel * † ‡ §, Christopher P. Kempes † ‡, and Sidney Redner † ¶ ‡

3 *School of Natural Science, University of California Merced, Merced, CA, †The Santa Fe Institute, Santa Fe, NM, ¶Department of Physics, Boston University, Boston
4 MA, ‡Contributed equally, and §To whom correspondence should be addressed: jdyeakel@gmail.com

5 Submitted to Proceedings of the National Academy of Sciences of the United States of America

6 The eco-evolutionary dynamics of species are fundamentally
7 linked to the energetic constraints of its constituent individuals.
8 Of particular importance are the tradeoffs between reproduction
9 and the dynamics of starvation and recovery in resource-limited
10 environments. To elucidate the consequences of this tradeoff,
11 we introduce a minimal nutritional state-structured model that in-
12 corporates two classes of consumer: nutritionally replete con-
13 sumers that reproduce, and undernourished, non-reproducing
14 consumers that are susceptible to mortality. As a function of the
15 transition rates between these replete and undernourished states
16 that are determined by the presence or absence of resources,
17 the consumer populations can either undergo cyclic dynamics or
18 reach a steady state. We obtain strong constraints on starvation
19 and recovery rates by deriving allometric scaling relationships
20 and find that population dynamics subject to these constraints
21 can approach the cyclic regime but are typically driven to a steady
22 state. Moreover, we find that these rates fall within a ‘refuge’ in pa-
23 rameter space, where the probability of extinction of the consumer
24 population is minimized. Thus we identify a potential mechanism
25 that may both drive and constrain the dynamics of animal pop-
26ulations. Our model provides a natural framework that predicts
27 maximum body size for mammals by determining the relative sta-
28 bility of an otherwise homogeneous population to a mutant pop-
29 ulation with altered percent body fat. For body masses $\lesssim 10^7$ g,
30 individuals with increased energetic reserves can invade resident
31 populations, and vice versa for body mass $\gtrsim 10^7$ g, thus providing
32 a principled mechanism for a within-lineage driver of Cope’s rule.

33 foraging | starvation | reproduction

34 **Significance Statement** Energetic investment in somatic mainte-
35 nance and growth vs. reproduction directly impacts the dynamics of
36 populations among species. Here, we construct a Nutritional State-
37 structured Model (NSM) to assess the population-level effects of star-
38 vation and recovery of a consumer population in a resource-limited en-
39 vironment, and use allometric scaling relationships for mammals to es-
40 tablish all timescales and rates. Our model reveals that mammalian
41 energetic rates minimize the probability of stochastic extinction, estab-
42 lishes dynamic bounds on mammalian body size while providing inde-
43 pendent theoretical support for the energy equivalence hypothesis, and
44 provides a mechanistic driver for the evolutionary trend towards larger
45 body size known as Cope’s rule.

46 Introduction

47 The behavioral ecology of all organisms is influenced by the en-
48 ergic state of individuals, which directly influences how they
49 invest reserves in uncertain environments. Such behaviors are
50 generally manifested as tradeoffs between investing in somatic
51 maintenance and growth, or allocating energy towards repro-
52 duction (1–3). The timing of these behaviors responds to se-
53 lective pressure, as the choice of the investment impacts future
54 fitness (4–6). The influence of resource limitation on an or-
55 ganism’s ability to maintain its nutritional stores may lead to
56 repeated delays or shifts in reproduction over the course of an
57 organism’s life.

58 The balance between (a) somatic growth and maintenance,
59 and (b) reproduction depends on resource availability (7). For
60 example, reindeer invest less in calves born after harsh winters
61 (when the mother’s energetic state is depleted) than in calves
62 born after moderate winters (8). Many bird species invest dif-
63 ferently in broods during periods of resource scarcity compared

64 to normal periods (9, 10), sometimes delaying or even foregoing
65 reproduction for a breeding season (1, 11, 12). Even fresh-
66 water and marine zooplankton have been observed to avoid
67 reproduction under nutritional stress (13), and those that do
68 reproduce have lower survival rates (2). Organisms may also
69 separate maintenance and growth from reproduction over space
70 and time: many salmonids, birds, and some mammals return to
71 migratory breeding grounds to reproduce after one or multiple
72 seasons in resource-rich environments where they accumulate
73 nutritional reserves (14–16).

74 Physiology also plays an important role in regulating repro-
75 ductive expenditures during periods of resource limitation. The
76 data collected thus far has shown that diverse mammals (47
77 species in 10 families) exhibit delayed implantation, whereby
78 females postpone fetal development (blastocyst implantation)
79 until nutritional reserves can be accumulated (17, 18). Many
80 other species (including humans) suffer irregular menstrual cy-
81 cling and higher abortion rates during periods of nutritional
82 stress (19, 20). In the extreme case of unicellular organisms,
83 nutrition is unavoidably linked to reproduction because the nu-
84 tritional state of the cell regulates all aspects of the cell cycle
85 (21). The existence of so many independently evolved mech-
86 anisms across such a diverse suite of organisms highlights the im-
87 portance and universality of the fundamental tradeoff between
88 somatic and reproductive investment. However the general dy-
89 namic implications of these constraints are unknown.

90 Though straightforward conceptually, incorporating the en-
91 ergic dynamics of individuals (22) into a population-level
92 framework (22, 23) presents numerous mathematical obsta-
93 cles (24). An alternative approach involves modeling the
94 macroscale relations that guide somatic versus reproductive
95 investment in a consumer-resource system. For example,
96 macroscale Lotka-Volterra models assume that the growth rate
97 of the consumer population depends on resource density, thus
98 implicitly incorporating the requirement of resource availability
99 for reproduction (25).

100 In this work, we adopt an alternative approach in which we
101 explicitly account for resource limitation and the subsequent
102 effects of starvation. Namely, only individuals with sufficient
103 energetic reserves can reproduce. Such a constraint leads to
104 reproductive time lags due to some members of the population
105 going hungry and then recovering. Additionally, we incorporate
106 the idea that reproduction is strongly constrained allometrically
107 (3), and is not generally linearly related to resource density. As
108 we shall show, these constraints influence the ensuing popula-

Reserved for Publication Footnotes

tion dynamics in dramatic ways.

Nutritional state-structured model (NSM)

We begin by defining a minimal Nutritional State-structured population Model (NSM), where the consumer population is partitioned into two states: (a) an energetically replete (full) state F , where the consumer reproduces at a constant rate λ and does not die from starvation, and (b) an energetically deficient (hungry) state H , where the consumer does not reproduce but dies by starvation at rate μ . The underlying resource R evolves by logistic growth with an intrinsic growth rate α and a carrying capacity C . The rate at which consumers transition between states and consume resources is dependent on their overall abundance, the abundance of resources, the efficiency of converting resources into metabolism, and how that metabolism is partitioned between maintenance and growth purposes. In the supplement we provide a fully mechanistic model for each of these dynamics and constants, and show that the system produces a simple non-dimensional form which we have described below (please see Supporting Information for a detailed derivation).

Consumers transition from the full state F to the hungry state H at a rate σ —the starvation rate—and also in proportion to the absence of resources ($1 - R$) (see Supporting Information for detailed a description and derivation of all rates). Conversely, consumers recover from state H to state F at rate $\xi\rho$ and in proportion to R , where ξ represents a ratio between maximal resource consumption and the carrying capacity of the resource. Resources are eaten by the consumers at rate $\rho R + \delta$, which accounts for somatic growth and maintenance for starving consumers, respectively, and at rate β by full consumers which is a constant representing maximal maintenance and somatic growth. The NSM represents a fundamental extension of the idealized starving random walk model of foraging, which focuses on resource depletion, to include reproduction and resource replenishment (26–28), and is a more general formulation than previous models incorporating starvation (29).

In the mean-field approximation, in which the consumers and resources are perfectly mixed, their densities evolve according to the rate equations

$$\begin{aligned}\dot{F} &= \lambda F + \xi\rho RH - \sigma(1 - R)F, \\ \dot{H} &= \sigma(1 - R)F - \xi\rho RH - \mu H, \\ \dot{R} &= \alpha R(1 - R) - (\rho R + \delta)H - \beta F\end{aligned}$$

This system of nondimensional equations follows from a set of first-principle relationships for resource consumption and growth (see Supplementary Materials for a full derivation and the dimensional form). Notice that the total consumer density $F + H$ evolves according to $\dot{F} + \dot{H} = \lambda F - \mu H$. This resembles the equation of motion for the predator density in the classic Lotka-Volterra model (30), except that the resource density does not appear in the growth term. As discussed above, the attributes of reproduction and mortality have been explicitly apportioned to the full and hungry consumers, respectively, so that the growth in the total density is decoupled from the resource density.

Equation [1] has three fixed points: two trivial fixed points at $(F^*, H^*, R^*) = (0, 0, 0)$ and $(0, 0, 1)$, and one non-trivial, internal fixed point at

$$\begin{aligned}F^* &= \frac{(\sigma - \lambda)\alpha\lambda\mu^2(\mu + \xi\rho)}{A(\lambda\rho B + \mu\sigma(\beta\mu + \lambda(\delta + \rho)))}, \\ H^* &= \frac{(\sigma - \lambda)\alpha\lambda^2\mu(\mu + \xi\rho)}{A(\lambda\rho B + \mu\sigma(\beta\mu + \lambda(\delta + \rho)))}, \\ R^* &= (\sigma - \lambda)\frac{\mu}{A}.\end{aligned}$$

where $A = (\lambda\xi\rho + \mu\sigma)$ and $B = (\beta\mu\xi + \delta\lambda\xi - \lambda\mu)$. The stability of this fixed point is determined by the Jacobian matrix \mathbf{J} , where each matrix element $J_{ij} = \partial\dot{X}_i/\partial X_j$ when evaluated at the internal fixed point, and \mathbf{X} is the vector (F, H, R) . The parameters in Eq. [1] are such that the real part of the largest eigenvalue of \mathbf{J} is negative, so that the system is stable with respect to small perturbations from the fixed point. Because this fixed point is unique, it is the global attractor for all population trajectories for any initial condition where the resource and consumer densities are both nonzero.

From Eq. [2], an obvious constraint on the NSM is that the reproduction rate λ must be less than the starvation rate σ , so that R^* is positive. In fact, when the resource density $R = 0$, the rate equation for F gives exponential growth of F for $\lambda > \sigma$. The condition $\sigma = \lambda$ represents a transcritical (TC) bifurcation (31) that demarcates the physical regime from the unphysical regime where all densities become < 0 . The biological implication of the constraint $\lambda < \sigma$ has a simple interpretation—the rate at which a macroscopic organism loses mass due to lack of resources is generally much faster than the rate of reproduction. As we will discuss below, this inequality is a natural consequence of allometric constraints (3) for organisms within empirically observed body size ranges.

In the physical regime of $\lambda < \sigma$, the fixed point [2] may either be a stable node or a limit cycle (Fig. 1). In continuous-time systems, a limit cycle arises when a pair of complex conjugate eigenvalues crosses the imaginary axis to attain positive real parts (32). This Hopf bifurcation is defined by $\text{Det}(\mathbf{S}) = 0$, with \mathbf{S} the Sylvester matrix, which is composed of the coefficients of the characteristic polynomial of the Jacobian matrix (33). As the system parameters are tuned to be within the stable regime but close to the Hopf bifurcation, the amplitude of the transient but decaying cycles become large. Given that ecological systems are constantly being perturbed (34), the onset of transient cycles, even though they decay with time in the mean-field description, can increase the extinction risk (35–37).

When the starvation rate $\sigma \gg \lambda$, a substantial fraction of the consumers are driven to the hungry non-reproducing state. Because reproduction is inhibited, there is a low steady-state consumer density and a high steady-state resource density. However, if $\sigma/\lambda \rightarrow 1$ from above, the population is overloaded with energetically-replete (reproducing) individuals, thereby promoting oscillations between the consumer and resource densities (Fig. 1).

Whereas the relation between consumer growth rate λ and the starvation rate σ defines an absolute bound of biological feasibility—the TC bifurcation— σ also determines the sensitivity of the consumer population to changes in resource density. When $\sigma \gg \lambda$, the steady-state population density is small, thereby increasing the risk of stochastic extinction. On the other hand, as σ decreases, the system will ultimately be poised either near the TC or the Hopf bifurcation (Fig. 1). If the recovery rate ρ is sufficiently small, the TC bifurcation is reached and the resource eventually is eliminated. If ρ exceeds a threshold value, cyclic dynamics will develop as the Hopf bifurcation is approached.

Role of allometry

While there are no a priori constraints on the parameters in the NSM, most organisms correspond to restricted portions of the parameter space. Here we use allometric scaling relations to constrain the covariation of rates in a principled and biologically meaningful manner. Allometric scaling relations highlight common constraints and average trends across large ranges in body size and species diversity. Many of these relations can be derived from a small set of assumptions and below we describe a

framework to determine the covariation of timescales and rates across the range of mammals for each of the key parameters of our model (cf. (38)). We are thereby able to define the regime of dynamics occupied by the entire class of mammals along with the key differences between the largest and smallest mammals.

Nearly all of the rates described in the NSM are determined by consumer metabolism, which can be used to describe a variety of organismal features (39). The scaling relation between an organism's metabolic rate B and its body mass M at reproductive maturity is known to scale as $B = B_0 M^\eta$ (40), where the scaling exponent η is typically close to 2/3 or 3/4 for metazoans (e.g., (39)), and has taxonomic shifts for unicellular species between $\eta \approx 1$ in eukaryotes and $\eta \approx 1.76$ in bacteria (3, 41).

Several efforts have shown how a partitioning of B between growth and maintenance purposes can be used to derive a general equation for both the growth trajectories and growth rates of organisms ranging from bacteria to metazoans (3, 42–45). This relation is derived from the simple balance condition

$$B_0 m^\eta = E_m \dot{m} + B_m m,$$

where E_m is the energy needed to synthesize a unit of mass, B_m is the metabolic rate to support an existing unit of mass, and m is the mass of the organism at any point in its development. This balance has the general solution (3, 46)

$$\left(\frac{m(t)}{M}\right)^{1-\eta} = 1 - \left[1 - \left(\frac{m_0}{M}\right)^{1-\eta}\right] e^{-a(1-\eta)t/M^{1-\eta}}, \quad [4]$$

where, for $\eta < 1$, $M = (B_0/B_m)^{1/(1-\eta)}$ is the asymptotic mass, $a = B_0/E_m$, and m_0 is mass at birth, itself varying allometrically as $9.7M^{0.92}$. We now use this solution to define the timescale of reproduction and recovery from starvation (Fig. 2; see (43) for a detailed presentation of these timescales). The time that it takes to reach a particular mass ϵM is given by the

$$\tau(\epsilon) = \ln \left[\frac{1 - (m_0/M)^{1-\eta}}{1 - \epsilon^{1-\eta}} \right] \frac{M^{1-\eta}}{a(1-\eta)}, \quad [5]$$

where we will define values of ϵ to describe a set of rates within our model. For the time to reproduce, $t_\lambda = \tau(\epsilon_\lambda)$, where ϵ_λ is the fraction of the asymptotic mass where an organism is reproductively mature and should be close to one (typically $\epsilon_\lambda \approx 0.95$ (42)). The growth rate is then given by $\lambda = \ln(v)/t_\lambda$ where v is the number of offspring produced, and for any constant value of ϵ_λ this will scale like $\lambda \propto M^{\eta-1}$ for $M \gg m_0$ (3, 42–45).

The rate of recovery $\rho = 1/t_\rho$ requires that an organism accrues sufficient tissue to transition from the hungry to the full state. Since only certain tissues can be digested for energy (for example the brain cannot be degraded to fuel metabolism), we define the rates for starvation, death, and recovery by the timescales required to reach, or return from, specific fractions of the replete-state mass (Fig. 3; see Supporting Information, Table I for parameterizations). We define $m_\sigma = \epsilon_\sigma M$, where $\epsilon_\sigma < 1$ is the fraction of replete-state mass where reproduction ceases. This fraction will be modified if tissue composition systematically scales with adult mass. For example, making use of the observation that body fat in mammals scales with overall body size according to $M_{\text{fat}} = f_0 M^\gamma$ and assuming that once this mass is fully digested the organism starves, this would imply that $\epsilon_\sigma = 1 - f_0 M^\gamma / M$. It follows that the recovery timescale, t_ρ , is the time to go from $m = \epsilon_\sigma \epsilon_\lambda M$ to $m = \epsilon_\lambda M$ (Fig. 2). Using Eqs. [4] and [5] this timescale is given by simply considering an adjusted starting mass of $m'_0 = \epsilon_\sigma \epsilon_\lambda M$, in which case

$$t_\rho = \ln \left[\frac{1 - (\epsilon_\sigma \epsilon_\lambda)^{1-\eta}}{1 - \epsilon^{1-\eta}} \right] \frac{M^{1-\eta}}{a'(1-\eta)} \quad [6]$$

$$\dot{m}E'_m = -B_m m \quad [7]$$

$$\dot{m} = -\frac{a'}{M^{1-\eta}} m \quad [8]$$

where E'_m is the amount of energy stored in a unit of existing body mass which differs from E_m , the energy required to synthesize a unit of biomass (45). Given the replete mass, M , of an organism, the above energy balance prescribes the mass trajectory of a non-consuming organism:

$$m(t) = M e^{-a't/M^{1-\eta}}. \quad [9]$$

The time scale for starvation is given by the time it takes $m(t)$ to reach $\epsilon_\sigma M$, which gives

$$t_\sigma = -\frac{M^{1-\eta}}{a'} \ln(\epsilon_\sigma). \quad [10]$$

The starvation rate is then $\sigma = 1/t_\sigma$, which scales with replete-state mass as $1/M^{1-\eta} \ln(1 - f_0 M^\gamma / M)$. An important feature is that σ does not have a simple scaling dependence on λ (Fig. 3), which is important for the dynamics that we later discuss.

The time to death should follow a similar relation, but defined by a lower fraction of replete-state mass, $m_\mu = \epsilon_\mu M$ where $\epsilon_\mu < \epsilon_\sigma$. Suppose, for example, that an organism dies once it has digested all fat and muscle tissues, and that muscle tissue scales with body mass according to $M_{\text{musc}} = u_0 M^\zeta$. This gives $\epsilon_\mu = 1 - (f_0 M^\gamma + u_0 M^\zeta) / M$. Muscle mass has been shown to be roughly proportional to body mass (47) in mammals and thus ϵ_μ is merely ϵ_σ minus a constant. The time to death is the total time to reach $\epsilon_\mu M$ minus the time to starve, or

$$t_\mu = -\frac{M^{1-\eta}}{a'} \ln(\epsilon_\mu) - t_\sigma, \quad [11]$$

and $\mu = 1/t_\mu$.

Although the rate equations [1] are general, here we focus on parameterizations for terrestrial-bound endotherms, specifically mammals, which range from a minimum of $M \approx 1\text{g}$ (the Etruscan shrew *Suncus etruscus*) to a maximum of $M \approx 10^7\text{g}$ (the late Eocene to early Miocene Indricotheriinae). Investigating other classes of organisms would simply involve altering the metabolic exponents and scalings associate with ϵ . Moreover, we emphasize that our allometric equations describe mean relationships, and do not account for the (sometimes considerable) variance associated with individual species.

Stabilizing effects of allometric constraints

As the allometric derivations of the NSM rate laws reveal, starvation and recovery rates are not independent parameters, and the biologically relevant portion of the phase space shown in

Fig. 1 is constrained via covarying parameters. Given the parameters of terrestrial endotherms, we find that the starvation rate σ and the recovery rate ρ are constrained to lie within a small window of potential values (Fig. 4) for the known range of body sizes M . We thus find that the dynamics for all mammalian body sizes are confined to the steady-state regime of the NSM and that limit-cycle behavior is precluded. Incorporating uncertainty in allometric parameters (20% variation around the mean; Fig. 4), we find that, for larger M , the distance to

the TC and Hopf bifurcation decreases. These results suggest that small mammals are marginally less prone to population oscillations—both stable limit cycles and transient cycles—than mammals with larger body size, though starvation and recovery rates across all values of M fall squarely in the steady state region at some distance from the Hopf bifurcation, suggesting that cyclic population dynamics should be rare, particularly in environments where resources are limiting.

It should be noted that previous studies have used allometric constraints to explain the periodicity of cyclic populations (48–50), suggesting a period $\propto M^{0.25}$. However this relation seems to hold only for some species (51), and potential drivers range from predator and/or prey lifespans to competitive dynamics (52, 53). Statistically significant support for the existence of population cycles among mammals is relatively rare though predominantly based on time series for small mammals (54). However the longer gestational times and increased difficulty in collecting adequate data precludes obtaining similar-quality information for larger organisms such that testing this particular result is not straightforward.

Extinction risk

Within our model, higher rates of starvation result in a larger flux of the population to the hungry state. In this state reproduction is absent, thus increasing the likelihood of extinction.

From the perspective of population survival, it is the rate of starvation relative to the rate of recovery that determines the long-term dynamics of the various species (Fig. 1). We therefore examine the competing effects of cyclic dynamics vs. changes in steady state density on extinction risk as a function of σ and ρ . To this end, we computed the probability of extinction, where we define extinction as a population trajectory falling below one fifth of the allometrically constrained steady state at any time between $t = 10^5$ and $t \leq 10^8$. This procedure is repeated for 50 replicates of the continuous-time system shown in Eq. 1 for an organism of $M = 100$ grams. In each replicate the initial densities are chosen to be (XF^*, XH^*, R^*) , with X a random variable that is uniformly distributed in $[0, 2]$. By allowing the rate of starvation to vary, we assessed extinction risk across a range of values for σ and ρ between ca. 10^{-7} to 10^{-3} . As expected, higher rates of extinction correlate with both high values of σ if ρ is small, and high values of ρ if σ is small. For low values of σ and high values of ρ , the increased extinction risk results from transient cycles with larger amplitudes as the system nears the Hopf bifurcation (Fig. 5). For high values of σ and low values of ρ , higher extinction risk arises because of the decrease in the steady state consumer population density (Figs. 1B, 5). This interplay creates an ‘extinction refuge’, such that for a constrained range of σ and ρ , extinction probabilities are minimized.

We find that the allometrically constrained values of σ and ρ fall squarely within the extinction refuge (Fig. 5, white point). These values are close enough to the Hopf bifurcation to avoid low steady state densities, and far enough away to avoid large-amplitude transient cycles. The fact that allometric values of σ and ρ fall within this relatively small window supports the possibility that a selective mechanism has constrained the physiological conditions that drive starvation and recovery rates within

populations. Such a mechanism would select for organism physiology that generates appropriate σ and ρ values that serve to minimize extinction risk. This selection could occur via the tuning of body fat percentages, metabolic rates, and biomass maintenance efficiencies. To summarize, our finding that the allometrically-determined parameters fall within this low extinction probability region suggests that the NSM dynamics may both drive—and constrain—natural animal populations.

Dynamic and energetic barriers to body size
Metabolite transport constraints are widely thought to place strict boundaries on biological scaling (39, 55, 56) and thereby lead to specific predictions on the minimum possible body size for organisms (57). Above this bound, a number of energetic and evolutionary mechanisms have been explored to assess the costs and benefits associated with larger body masses, particularly for mammals. One important such example is the *fast-ing endurance hypothesis*, which contends that larger body size, with consequent lower metabolic rates and increased ability to maintain more endogenous energetic reserves, may buffer organisms against environmental fluctuations in resource availability (58). Over evolutionary time, terrestrial mammalian lineages show a significant trend towards larger body size (known as Cope’s rule) (59–62), and it is thought that within-lineage drivers generate selection towards an optimal upper bound of roughly 10^7 grams (59), a value that is likely limited by higher extinction risk for large taxa over longer timescales (60). These trends are thought to be driven by a combination of climate change and niche availability (62); however the underpinning energetic costs and benefits of larger body sizes, and how they influence dynamics over ecological timescales, have not been explored. We argue that the NSM provides a suitable framework to explore these issues.

The NSM correctly predicts that species with smaller masses have larger steady-state population densities (Fig. 6A). Moreover, we show that the NSM provides independent theoretical support for the energy equivalence hypothesis (63, 64). The energy equivalence hypothesis argues that the total energy use, B_{tot} , of a population is constant independent of species size (e.g. (63, 64)). This hypothesis is based on observations showing that the steady state abundance, N^* , of a species is proportional to the inverse of individual metabolism (e.g. $N^* \propto M^{-3/4}/B_0$) (e.g. (63, 64)). This is usually stated as $B_{\text{tot}} = N^* B(M) = Q$ where Q is a constant, and has been shown to hold in both mammalian and vascular plant communities (63, 64). Figure 6A shows that both F^* and H^* scale like $M^{-\eta}$ over a wide range of organism sizes and Figure 6B shows that $F^* B$ is nearly constant over this same range. This result is remarkable because it illustrates that the steady state values of the NSM combined with the derived timescales naturally give rise to the energy equivalence result. Our model shows that the equivalence breaks down at the maximum observed body sizes for mammals, suggesting that this is a hard limit where deviations outside of this range are energetically suboptimal. In the framework of our model, the total metabolic rate of F and H becomes infinite at a finite mass, occurring at the same scale where the steady state resources vanish (Fig. 6). This asymptotic behavior represents an upper bound on mammalian body size and occurs at $M_{\text{max}} = 6.5 \times 10^7$. Moreover, M_{max} , which is entirely determined by the population-level consequences of energetic constraints, is remarkably close to the maximum body size observed in the North American mammalian fossil record (59) as well as the mass predicted from an evolutionary model of body size evolution (60). We note that the prediction of an asymptotic limit on mammalian size parallels work on microbial life where an upper and lower bound on bacterial size, and an upper

462 bound on single cell eukaryotic size, is predicted from similar 526 in the NSM may provide a general within-lineage mechanism
 463 growth and energetic scaling relationships (3, 65). 527 for the evolution of larger body size among terrestrial mammals.
 464 We contend that the NSM provides a mechanistic under- 528 The energetics associated with somatic maintenance,
 465 standing of the energetic dynamics that give rise to both ob- 529 growth, and reproduction are important elements that influence
 466 served limitations on mammalian body size as well as the ob- 530 the dynamics of all populations (11). The NSM is a minimal
 467 served trend towards larger body size over evolutionary time. 531 and general model that incorporates the dynamics of starvation
 468 The NSM predicts that the steady state resource density R^* 532 and recovery that are expected to occur in resource-limited en-
 469 decreases with increasing body size of the consumer popula- 533 vironments. By incorporating allometric relations between the
 470 tion (Fig. 6C), and classic resource competition theory predicts 534 rates in the NSM, we found: (i) different organismal masses
 471 that the species surviving on the lowest resource abundance will 535 have distinct population dynamic regimes, (ii) allometrically-
 472 outcompete others (66–68). Thus, the combined NSM steady- 536 determined rates of starvation and recovery appear to minimize
 473 state dynamics and allometric timescales predict that larger 537 extinction risk, and (iii) the dynamic consequences of these rates
 474 mammals have an intrinsic competitive advantage given a com- 538 may introduce additional drivers and hard boundaries on the
 475 mon resource, but does not offer a within-lineage mechanism by 539 evolution of maximum body size. We suggest that the NSM
 476 which larger body sizes are selected for. 540 offers a means by which the dynamic consequences of energetic
 477 To examine whether the NSM could provide such a mecha- 541 constraints can be assessed using macroscale interactions be-
 478 nism, we begin by noting that a theoretical upper bound on 542 tween and among species. Future efforts will involve exploring
 479 mammalian body size is given by $\epsilon_\sigma = 0$, where mammals 543 the consequences of these dynamics in a spatially explicit frame-
 480 are entirely composed of metabolic reserves, and this occurs at 544 work, thus incorporating elements such as movement costs and
 481 $M = 8.3 \times 10^8$, or $120 \times$ the mass of a male African elephant. 545 spatial heterogeneity, which may elucidate additional tradeoffs
 482 Next we examine to what extent a more realistic upper bound 546 associated with the dynamics of starvation and recovery.
 483 to body mass may serve as an evolutionary attractor, thus pro-
 484 viding a suitable within-lineage mechanism for Cope's rule. We
 485 directly assess the susceptibility of an otherwise homogeneous
 486 population to invasion by a mutated subset of the population
 487 (denoted by ') where individuals have a modified proportion of
 488 body fat $M' = M(1 + \chi)$ where $\chi \in [-f_0 M^{\gamma-1}, 0.05]$ (where
 489 the lower bound of χ is the proportion of body mass that is
 490 not composed of metabolic reserves and the upper bound main-
 491 tains the organism's reproductive mass), thus altering the rates
 492 of starvation $\sigma(M')$, recovery $\rho(M')$, and the maintenance of
 493 both starving $\delta(M')$ and full consumers $\beta(M')$. Importantly,
 494 ϵ_σ , which determines the point along the growth curve the de-
 495 fines the state of starved foragers, is assumed to remain un-
 496 changed for the invader population (see Supplemental Material
 497 for detailed derivations of invader rates).

498 To assess the susceptibility of the resident population to
 499 invasion, we determine which consumer has a lower steady-
 500 state resource density for a given value of χ , again with the
 501 expectation that populations able to survive on lower resource
 502 densities have a competitive advantage (66). We find that for
 503 $M \leq 1.73 \times 10^7$ g, having additional body fat ($\chi > 0$) results in
 504 lower steady state resource density ($R^* < R'$), such that the
 505 invader has an intrinsic competitive advantage over the resident
 506 population. However, for $M > 1.73 \times 10^7$ g, leaner individuals
 507 ($\chi < 0$) have lower resource steady state densities, switching
 508 the advantage for higher values of M .

509 The observed switch in susceptibility as a function of χ at
 510 $M_{\text{opt}} = 1.73 \times 10^7$ g thus serves as an attractor, such that the
 511 NSM predicts organismal mass to increase if $M < M_{\text{opt}}$ and
 512 decrease if $M > M_{\text{opt}}$. This value is close to but smaller than
 513 the asymptotic upper bound for terrestrial mammal body size
 514 predicted by the NSM, however it is remarkably close to in-
 515 dependent estimates of the largest land mammals, the early
 516 Oligocene *Indricotherium* at ca. 1.3×10^7 g and the late Miocene
 517 *Deinotherium* at ca. 1.74×10^7 g (61). Additionally, our calcula-
 518 tion of M_{opt} as a function of mass-dependent physiological rates
 519 is similar to theoretical estimates of maximum body size (60),
 520 and provides independent theoretical support for the observa-
 521 tion of a 'maximum body size attractor' for North American
 522 mammals outlined by Alroy (59). While the state of the envi-
 523 ronment, as well as the competitive landscape, will determine
 524 whether specific body sizes are selected for or against (62), we
 525 propose that the dynamics of starvation and recovery described

526 in the NSM may provide a general within-lineage mechanism
 527 for the evolution of larger body size among terrestrial mammals.
 528 The energetics associated with somatic maintenance,
 529 growth, and reproduction are important elements that influence
 530 the dynamics of all populations (11). The NSM is a minimal
 531 and general model that incorporates the dynamics of starvation
 532 and recovery that are expected to occur in resource-limited en-
 533 vironments. By incorporating allometric relations between the
 534 rates in the NSM, we found: (i) different organismal masses
 535 have distinct population dynamic regimes, (ii) allometrically-
 536 determined rates of starvation and recovery appear to minimize
 537 extinction risk, and (iii) the dynamic consequences of these rates
 538 may introduce additional drivers and hard boundaries on the
 539 evolution of maximum body size. We suggest that the NSM
 540 offers a means by which the dynamic consequences of energetic
 541 constraints can be assessed using macroscale interactions be-
 542 tween and among species. Future efforts will involve exploring
 543 the consequences of these dynamics in a spatially explicit frame-
 544 work, thus incorporating elements such as movement costs and
 545 spatial heterogeneity, which may elucidate additional tradeoffs
 546 associated with the dynamics of starvation and recovery.

References

1. Martin TE (1987) Food as a Limit on Breeding Birds: A Life-History Perspective. *Annu. Rev. Ecol. Syst.* 18:453–487.
2. Kirk KL (1997) Life-History Responses to Variable Environments: Starvation and Reproduction in Planktonic Rotifers. *Ecology* 78:434–441.
3. Kempes CP, Dutkiewicz S, Follows MJ (2012) Growth, metabolic partitioning, and the size of microorganisms. *PNAS* 109:495–500.
4. Mangel M, Clark CW (1988) *Dynamic Modeling in Behavioral Ecology* (Princeton University Press, Princeton).
5. Mangel M (2014) Stochastic dynamic programming illuminates the link between environment, physiology, and evolution. *B. Math. Biol.* 77:857–877.
6. Yeakel JD, Dominy NJ, Koch PL, Mangel M (2014) Functional morphology, stable isotopes, and human evolution: a model of consilience. *Evolution* 68:190–203.
7. Morris DW (1987) Optimal Allocation of Parental Investment. *Oikos* 49:332.
8. Tveraa T, Fauchald P, Henaug C, Yoccoz NG (2003) An examination of a compensatory relationship between food limitation and predation in semi-domestic reindeer. *Oecologia* 137:370–376.
9. Daan S, Dijkstra C, Drent R, Meijer T (1988) *Food supply and the annual timing of avian reproduction*.
10. Jacot A, Valcu M, van Oers K, Kempenaers B (2009) Experimental nest site limitation affects reproductive strategies and parental investment in a hole-nesting passerine. *Animal Behaviour* 77:1075–1083.
11. Stearns SC (1989) Trade-Offs in Life-History Evolution. *Funct. Ecol.* 3:259.
12. Barboza P, Jorde D (2002) Intermittent fasting during winter and spring affects body composition and reproduction of a migratory duck. *J Comp Physiol B* 172:419–434.
13. Threlkeld ST (1976) Starvation and the size structure of zooplankton communities. *Freshwater Biol.* 6:489–496.
14. Weber TP, Ens BJ, Houston AI (1998) Optimal avian migration: A dynamic model of fuel stores and site use. *Evolutionary Ecology* 12:377–401.
15. Mduma SAR, Sinclair ARE, Hilborn R (1999) Food regulates the Serengeti wildebeest: a 40-year record. *J. Anim. Ecol.* 68:1101–1122.

- 590 16. Moore JW, Yeakel JD, Peard D, Lough J, Beere M (2014) 657
 591 Life-history diversity and its importance to population sta- 658 41. DeLong JP, Okie JG, Moses ME, Sibly RM, Brown JH
 592 bility and persistence of a migratory fish: steelhead in two 659 (2010) Shifts in metabolic scaling, production, and effi-
 593 large North American watersheds. *J. Anim. Ecol.* 83:1035– 660 ciency across major evolutionary transitions of life. *PNAS*
 594 1046. 661 107:12941–12945.
 595 17. Mead RA (1989) in *Carnivore Behavior, Ecology, and Evo-* 662 42. West GB, Brown JH, Enquist BJ (2001) A general model
 596 *lution* (Springer US, Boston, MA), pp 437–464. 663 for ontogenetic growth. *Nature* 413:628–631.
 597 18. Sandell M (1990) The Evolution of Seasonal Delayed Im- 664 43. Moses ME, et al. (2008) Revisiting a Model of Ontogenetic
 598 plantation. *The Quarterly Review of Biology* 65:23–42. 665 Growth: Estimating Model Parameters from Theory and
 599 19. Bulik CM, et al. (1999) Fertility and Reproduction in 666 Data. <http://dx.doi.org.proxy.lib.sfu.ca/10.1086/679735>
 600 Women With Anorexia Nervosa. *J. Clin. Psychiatry* 667 171:632–645.
 601 60:130–135.
 602 20. Trites AW, Donnelly CP (2003) The decline of Steller sea 668 44. Gillooly JF, Charnov EL, West GB, Savage VM, Brown JH
 603 lions *Eumetopias jubatus* in Alaska: a review of the nutri- 669 (2002) Effects of size and temperature on developmental
 604 tional stress hypothesis. *Mammal Review* 33:3–28. 670 time. *Nature* 417:70–73.
 605 21. Glazier DS (2009) Metabolic level and size scaling of rates 671 45. Hou C, et al. (2008) Energy Uptake and Allocation During
 606 of respiration and growth in unicellular organisms. *Funct. 672 Ontogeny. *Science* 322:736–739.
 607 *Ecol.* 23:963–968. 673 46. Bettencourt LMA, Lobo J, Helbing D, Kuhnert C, West
 608 22. Kooijman SALM (2000) *Dynamic Energy and Mass Bud- 674 GB (2007) Growth, innovation, scaling, and the pace of life
 609 gets in Biological Systems* (Cambridge). 675 in cities. *Proc. Natl. Acad. Sci. USA* 104:7301–7306.
 610 23. Sousa T, Domingos T, Poggiale JC, Kooijman SALM 676 47. Folland JP, Mc Cauley TM, Williams AG (2008) Allometric
 611 (2010) Dynamic energy budget theory restores coherence 677 scaling of strength measurements to body size. *Eur J
 612 in biology. *Philos. T. Roy. Soc. B* 365:3413–3428. 678 *Appl Physiol* 102:739–745.
 613 24. Diekmann O, Metz JAJ (2010) How to lift a model for in- 679 48. Calder III WA (1983) An allometric approach to population
 614 dividual behaviour to the population level? *Philos. T. Roy. 680 cycles of mammals. *J. Theor. Biol.* 100:275–282.
 615 *Soc. B* 365:3523–3530. 681 49. Peterson RO, Page RE, Dodge KM (1984) Wolves, Moose,
 616 25. Murdoch WW, Briggs CJ, Nisbet RM (2003) *Consumer- 682 and the Allometry of Population Cycles. *Science* 224:1350–
 617 resource Dynamics*, Monographs in population biology 683 1352.
 618 (Princeton University Press). 684 50. Krukonis G, Schaffer WM (1991) Population cycles in mam-
 619 26. Benichou O, Redner S (2014) Depletion-Controlled Starva- 685 mals and birds: Does periodicity scale with body size? *J.
 620 tion of a Diffusing Forager. *arXiv*. 686 *Theor. Biol.* 148:469–493.
 621 27. Bénichou O, Chupeau M, Redner S (2016) Role of Deple- 687 51. Hendriks AJ, Mulder C (2012) Delayed logistic and Rosen-
 622 tion on the Dynamics of a Diffusing Forager. 688 zweig–MacArthur models with allometric parameter setting
 623 28. Chupeau M, Bénichou O, Redner S (2016) Universality 689 estimate population cycles at lower trophic levels well. *Eco-
 624 classes of foraging with resource renewal. *Phys. Rev. E* 690 9:43–54.
 625 93:032403. 691 52. Kendall BE, et al. (1999) Why do populations cycle? A syn-
 626 29. Persson L, Leonardsson K, De Roos AM, Gyllenberg M, 692 thesis of statistical and mechanistic modeling approaches.
 627 Christensen B (1998) Ontogenetic Scaling of Foraging Rates 693 *Ecology* 80:1789–1805.
 628 and the Dynamics of a Size-Structured Consumer-Resource 694 53. Höglstedt G, Seldal T, Breistøl A (2005) Period length in
 629 Model. *Theoretical Population Biology* 54:270–293. 695 cyclic animal populations. *Ecology* 86:373–378.
 630 30. Murray JD (2011) *Mathematical Biology: I. An Introduct-* 696 54. Kendall, Prendergast, Bjornstad (1998) The macroecology
 631 *tion, Interdisciplinary Applied Mathematics* (Springer New 697 of population dynamics: taxonomic and biogeographic pat-
 632 York) Vol. 110. 698 terns in population cycles. *Ecol. Lett.* 1:160–164.
 633 31. Strogatz SH (2008) *Nonlinear Dynamics and Chaos, With 699 55. Brown J, Marquet P, Taper M (1993) Evolution of body
 634 Applications to Physics, Biology, Chemistry, and Engineer- 700 size: consequences of an energetic definition of fitness. *Am.
 635 ing* (Westview Press). 701 *Nat.* 142:573–584.
 636 32. Guckenheimer J, Holmes P (1983) *Nonlinear oscilla- 702 56. West GB, Brown JH, Enquist BJ (1997) A General Model
 637 tions, dynamical systems, and bifurcations of vector fields* 703 for the Origin of Allometric Scaling Laws in Biology. *Sci-
 638 (Springer, New York). 704 ence* 276:122–126.
 639 33. Gross T, Feudel U (2004) Analytical search for bifurcation 705 57. West GB, Woodruff WH, Brown JH (2002) Allometric scal-
 640 surfaces in parameter space. *Physica D* 195:292–302. 706 ing of metabolic rate from molecules and mitochondria to
 641 34. Hastings A (2001) Transient dynamics and persistence of 707 cells and mammals. *Proc. Natl. Acad. Sci. USA* 99:2473–
 642 ecological systems. *Ecol. Lett.* 4:215–220. 708 2478.
 643 35. Neubert M, Caswell H (1997) Alternatives to resilience for 709 58. Millar J, Hickling G (1990) Fasting Endurance and the
 644 measuring the responses of ecological systems to perturba- 710 Evolution of Mammalian Body Size. *Funct. Ecol.* 4:5–12.
 645 tions. *Ecology* 78:653–665. 711 59. Alroy J (1998) Cope's rule and the dynamics of body
 646 36. Caswell H, Neubert MG (2005) Reactivity and transient 712 mass evolution in North American fossil mammals. *Science*
 647 dynamics of discrete-time ecological systems. *Journal of 713 280:731.
 648 Difference Equations and Applications* 11:295–310. 714 60. Clauset A, Redner S (2009) Evolutionary Model of Species
 649 37. Neubert M, Caswell H (2009) Detecting reactivity. *Ecology* 715 Body Mass Diversification. *Phys. Rev. Lett.* 102:038103.
 650 38. Yodzis P, Innes S (1992) Body Size and Consumer-Resource 716 61. Smith FA, et al. (2010) The Evolution of Maximum Body
 651 Dynamics. *Am. Nat.* 139:1151–1175. 717 Size of Terrestrial Mammals. *Science* 330:1216–1219.
 652 39. Brown J, Gillooly J, Allen A, Savage V, West G (2004) To 718 62. Saarinen JJ, et al. (2014) Patterns of maximum body size
 653 ward a metabolic theory of ecology. *Ecology* 85:1771–1789. 719 evolution in Cenozoic land mammals: eco-evolutionary pro-
 654 40. West GB, Woodruff WH, Brown JH (2002) Allometric scal- 720 720 cesses and abiotic forcing. *Proc Biol Sci* 281:20132049–
 655 ing of metabolic rate from molecules and mitochondria to 721 20132049.
 656 cells and mammals. *Proc. Natl. Acad. Sci. USA* 99 Suppl 722 63. Allen AP, Brown JH, Gillooly JF (2002) Global Biodiver-
 723 sity, Biochemical Kinetics, and the Energetic-Equivalence******

- 724 Rule. *Science* 297:1545–1548.
- 725 64. Enquist BJ, Brown JH, West GB (1998) Allometric scal- 736 *geochem. Cycles* 23:1–15.
- 726 ing of plant energetics and population density : Abstract : 737 68. Barton AD, Dutkiewicz S, Flierl G, Bragg J, Follows MJ
- 727 Nature. *Nature* 395:163–165. 738 (2010) Patterns of Diversity in Marine Phytoplankton. *Sci-*
- 728 65. Kempes CP, Wang L, Amend JP, Doyle J, Hoehler T (2016) 739 *ence* 327:1509–1511.
- 729 Evolutionary tradeoffs in cellular composition across diverse 740 **ACKNOWLEDGMENTS.** We thank Luis Bettencourt, Jean Philippe Gibert,
- 730 bacteria. *ISME J* 10:2145–2157. 741 Eric Libby, and Seth Newsome for helpful discussions and comments on the
- 731 66. Tilman D (1981) Tests of Resource Competition Theory Us- 742 manuscript. J.D.Y. was supported by startup funds at the University of California,
- 732 ing Four Species of Lake Michigan Algae. *Ecology* 62:802– 743 Merced, and an Omidyar Postdoctoral Fellowship at the Santa Fe Institute. C.P.K.
- 733 815. 744 was supported by an Omidyar Postdoctoral Fellowship at the Santa Fe Institute.
- 734 67. Dutkiewicz S, Follows MJ, Bragg JG (2009) Modeling the 745 S.R. was supported by grants DMR-1608211 and 1623243 from the National
- 735 coupling of ocean ecology and biogeochemistry. *Global Bio- 746 Science Foundation, and by the John Templeton Foundation, all at the Santa Fe*
- 747 *Institute.*

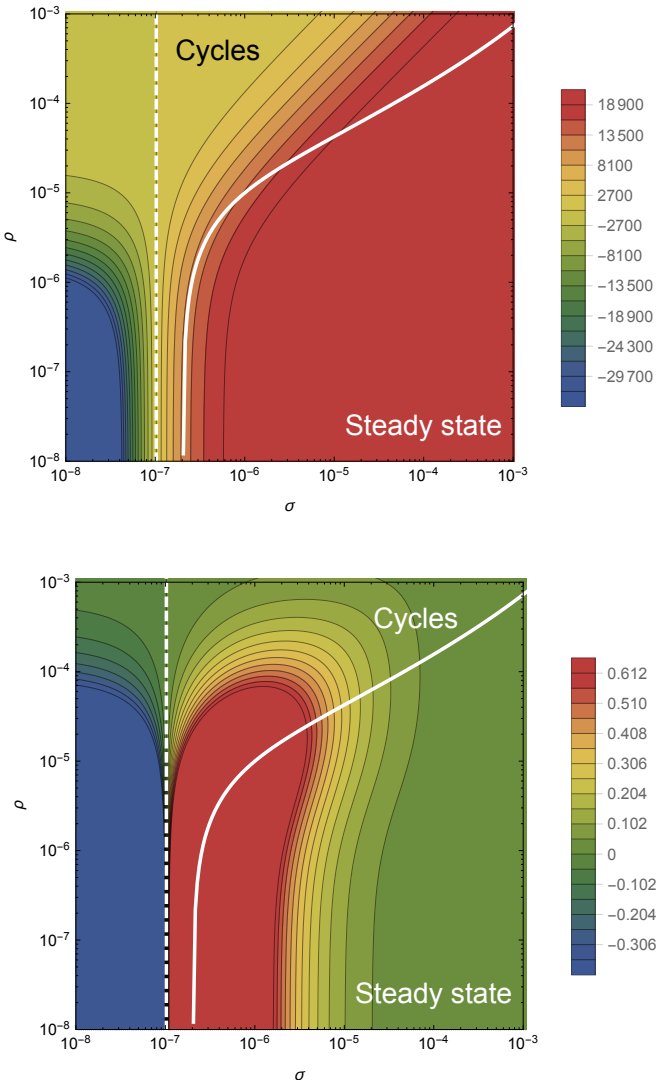


Fig. 1: The transcritical (dashed) and Hopf bifurcation (solid) as a function of the starvation rate σ and recovery rate ρ for a 100g consumer. These bifurcation conditions separate parameter space into infeasible, cyclic, and steady state dynamic regimes. The color gradient shows the steady state densities for (A) the resource R^* and the (B) energetically replete consumers F^* , (warmer colors denote higher densities). Steady state densities for the energetically deficient consumers H^* (not shown) scale with those for F^* .

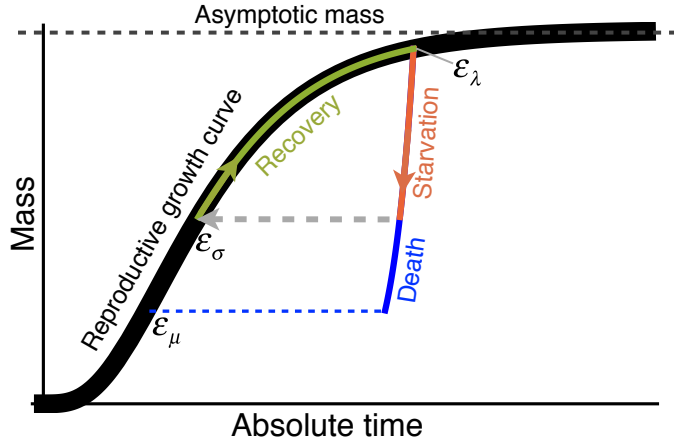


Fig. 2: The growth trajectory over absolute time of an individual organism as a function of body mass. Initial growth follows the black trajectory to an energetically replete reproductive adult mass $m = \epsilon_\lambda M$ which we assume is 95% asymptotic mass M . Starvation follows the red trajectory to $m = \epsilon_\sigma \epsilon_\lambda M$, and recovery follows the green growth trajectory to the replete adult mass. Alternatively, death from starvation follows the blue trajectory to $m = \epsilon_\mu \epsilon_\lambda M$.

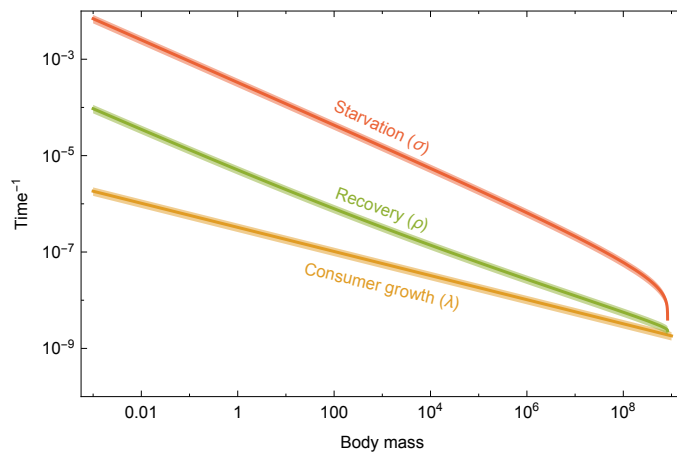


Fig. 3: Allometrically constrained starvation rate σ (red) and recovery rate ρ (green) relative to the reproductive rate λ (orange) as a function of body mass. The rate of starvation is greater than the rate of reproduction for all realized terrestrial endotherm body sizes. Mean values $\pm 20\%$ variation are shown by the shaded region for each rate.

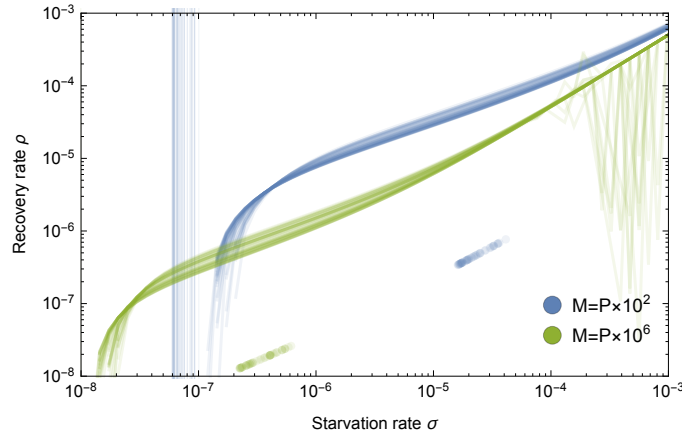


Fig. 4: Transcritical (vertical lines) and Hopf bifurcations (curves) for allometrically determined starvation σ and recovery ρ rates as a function of different mammalian body sizes: $M = P \times 10^2\text{g}$ (blue) and $M = P \times 10^6\text{g}$ (green), where P is a random uniform variable in $[1, 9]$. Points denote realized values of σ and ρ given the drawn values for M .

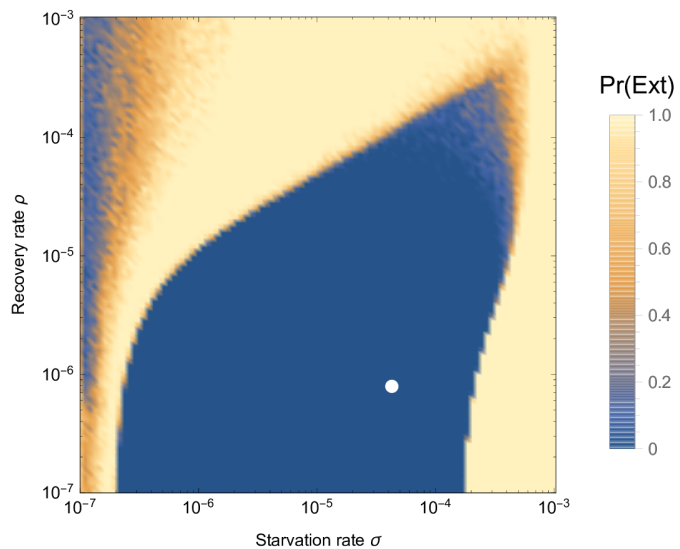


Fig. 5: Probability of extinction for a 100g consumer as a function of the starvation rate σ and recovery rate ρ , where the initial density is given as $A(F^*, H^*, R^*)$, with A being a random uniform variable in $[0, 2]$. Extinction is defined as the population trajectory falling below $0.1 \times$ the allometrically constrained steady state. The white point denotes the allometrically constrained starvation and recovery rate.

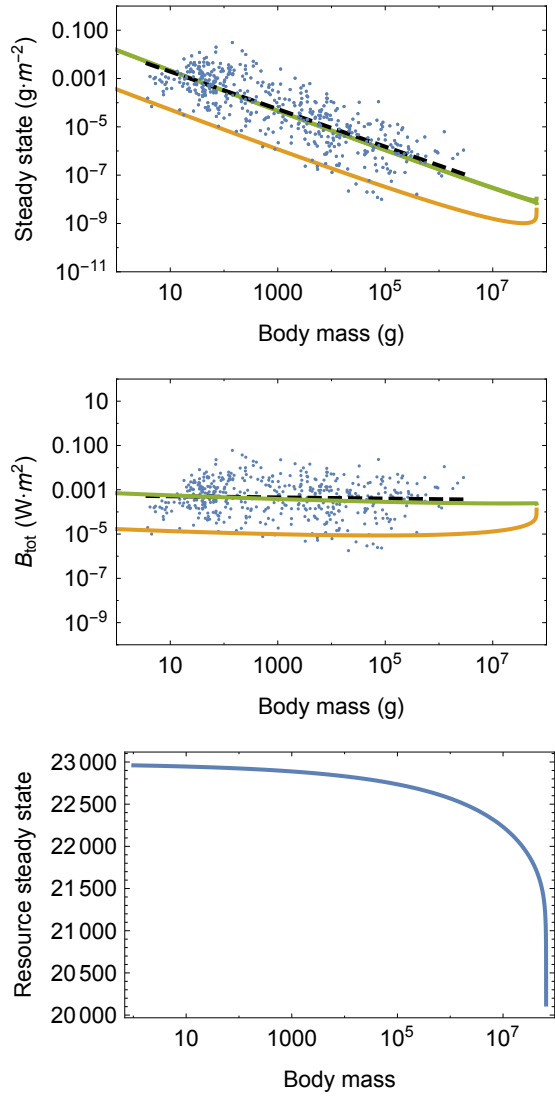


Fig. 6: (A) Consumer steady states F^* (green) and H^* (orange) as a function of body mass. (B) Total energetic use B_{tot} of consumer populations at the steady state as a function of body mass. (C) Resource steady state R^* as a function of consumer body mass.

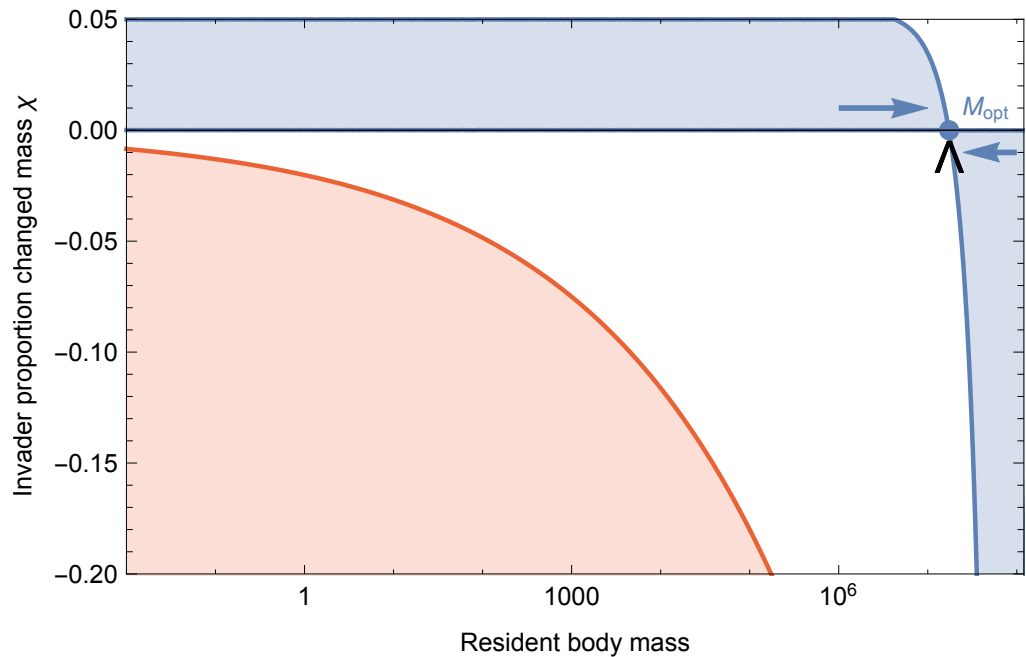


Fig. 7: Invasion feasibility for organisms with a proportional change in mass χ against a population with a resident body mass M . The blue region denotes proportions of modified mass χ resulting in successful invasion. The red region denotes values of χ that result in a mass that is below the starvation threshold and is thus infeasible. Arrows point to the predicted optimal mass $M_{\text{opt}} = 1.73 \times 10^7$, which serves as an evolutionary attractor for body mass. The black wedge points to the largest body mass known for terrestrial mammals at 7.74×10^7 g (61).